RECONSTRUCTION ALGORITHMS FOR AN INVERSE MEDIUM PROBLEM

Ji-Chuan Liu, Jiangsu

Received April 27, 2017. First published March 20, 2018.

Abstract. In this paper, we consider a two-dimensional inverse medium problem from noisy observation data. We propose effective reconstruction algorithms to detect the number, the location and the size of the piecewise constant medium within a body, and then we try to recover the unknown shape of inhomogeneous media. This problem is nonlinear and ill-posed, thus we should consider stable and elegant approaches in order to improve the corresponding approximation. We give several examples to show the viability of our proposed algorithms.

Keywords: inverse medium problem; Levenberg-Marquardt algorithm; trust-region-reflective algorithm; ill-posed problem

MSC 2010: 65N20, 65N21

1. Introduction

We consider an inverse medium problem to reconstruct the salient features of inhomogeneous media within a body from the internal measured data which arises from the problem of microwave imaging of biological tissue [3], [4], [6], [7], [8], [5], [26]. The objective is to stabilize and improve the resolution and contrast of imaging of biological tissues, while reducing the costs. This inverse medium problem is known to be ill-posed [14], [16], [24], that is, any small change of the measured data can result in a dramatic change of the inhomogeneous medium. Thus we should use regularization techniques to deal with this inverse medium problem.

Reconstruction algorithms of inverse medium problems have been introduced and studied over the last decade [2], [4], [9], [10], [17], [23], [25]. Ammari et al. [4] extended the method developed by Ammari et al. in [1] to reliably reconstruct both

The research was supported by the NSF of China (11601512, 11326236) and the Fundamental Research Funds for the Central Universities (2014QNA57).

the real-valued functions a and q from the internal energies. Choulli and Triki [10] proposed new weighted stability estimates for the inverse medium problem with internal data. Triki [25] studied the uniqueness of the inverse medium problem with internal data and got a local Lipschitz stability of the reconstruction. Ammari et al. [2] provided an iterative algorithm for reconstructing the optical absorption coefficient and proved the convergence of the algorithm. Schotland [23] employed various direct reconstruction algorithms to reconstruct the optical properties of a medium of interest from boundary measurements within a body. Bao and Triki [9] proposed a general recursive linearization algorithm to solve inverse medium problems from multi-frequency measurements. Ito et al. [17] presented a novel sampling method for time harmonic inverse medium scattering problems.

In this paper, we study an inverse medium problem where the inhomogeneous medium to be recovered consists of piecewise constant parts within a body. Then this inverse medium problem can be transformed into a transmission problem. Based on the fundamental solution of Helmholtz equation, we can obtain the expression of solution for the transmission problem with boundary integral equations. This inverse medium problem is nonlinear and ill-posed. Thus we employ iterative regularization algorithms to solve this inverse medium problem. We propose Trust-Region-Reflective algorithm (TRA) and Levenberg-Marquardt algorithm (LMA) to detect the number, the location and the size, and then to recover the shape of inhomogeneous media within a body. Numerical experiments show that the proposed algorithms are feasible and stable to determine the salient features of inhomogeneous media from boundary measurements.

The outline of the paper is as follows. In Section 2, we introduce an inverse medium problem. In Section 3, we present the parameterization of the boundary of the inhomogeneous medium. We propose reconstruction algorithms to solve the inverse medium problem in Section 4. Numerical experiments are presented in Section 5 to illustrate the efficiency of the proposed algorithms. Finally, we give some concluding remarks in Section 6.

2. Formulation of an inverse medium problem

Our goal is to numerically study a time harmonic inverse medium problem. Let Ω be a simply connected bounded domain with boundary of class C^2 and q a positive and piecewise constant function in Ω. For the boundary data $f \in H^{1/2}(\partial\Omega)$, we consider the Helmholtz equation

$$\begin{cases} \Delta u + qu = 0 & \text{in } \Omega, \\ u = f & \text{on } \partial\Omega, \end{cases} \tag{1}$$

where Δ is the Laplacian. Assume 0 is not in the spectrum of $\Delta + q$ with the solution domain $H_0^1(\Omega) \cap H^2(\Omega)$. If q and f are known, it is well known that there exists a unique $u \in H^1(\Omega)$, the solution to problem (1), see [21], [25].

According to a given Dirichlet data f, the inverse medium problem consists of reconstructing q in Ω from Neumann boundary condition

$$\frac{\partial u}{\partial \nu} = g \quad \text{on } \partial\Omega, \tag{2}$$

where ν is the outward unit normal to the boundary $\partial\Omega$. Furthermore, q is a piecewise constant function in Ω, which means that a bounded domain Ω in the homogeneous background space is occupied by some inhomogeneous media. In this paper, we want to seek effective and stable algorithms to determine the salient features of the inhomogeneous media.

Provided q is piecewise constant, the inverse medium problem simplifies into an inverse transmission problem with the boundaries of the unknown inhomogeneous media. We denote the boundary of Ω by $\Gamma_0 := \partial\Omega$. Assume that $\Omega_1, \ldots, \Omega_N$ are N starlike simply connected subdomains contained in Ω, the closures of which are pairwise disjoint, denote the boundary of Ω_k by Γ_k for $k = 1, \ldots, N$, and set $\Omega_0 = \Omega \setminus \bigcup_{k=1}^{N} \Omega_k$. We denote by ν the outward unit normal to each of the curves Γ_k for $k = 0, 1, \ldots, N$. Let $q|_{\Omega_k} = q_k$ for $k = 0, 1, \ldots, N$. Figure 1 shows an example with $N = 2$.

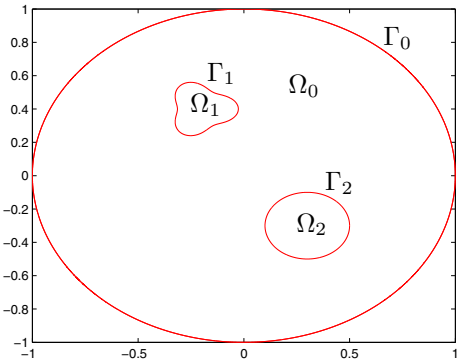

Figure 1. Example of a configuration Ω.

Because of q being piecewise constant, the problem (1) is equivalent to finding a set of coupled Helmholtz equations

$$\Delta u_k + q_k u_k = 0, \quad \text{in } \Omega_k, \ k = 0, 1, \ldots, N, \tag{3}$$

satisfying interface conditions

$$\begin{cases} u_0 = f & \text{on } \Gamma_0, \\ u_0 = u_k & \text{on } \Gamma_k, \\ \dfrac{\partial u_0}{\partial \nu} = \dfrac{\partial u_k}{\partial \nu} & \text{on } \Gamma_k. \end{cases} \tag{4}$$

From [21], [25], we know that (3)–(4) have a unique solution $u \in H^1(\Omega)$ along with q and f known. To our knowledge, we can use single- and double-layer potentials to find solutions to the Helmholtz equation in a bounded domain with a continuous density φ, see Chapter 3 of [14]. We denote the fundamental solution to the Helmholtz equation by

$$G_k(x,y) = \frac{\mathrm{i}}{4} H_0^{(1)}(\sqrt{q_k}|x-y|), \quad x \neq y,\ k = 0, 1, \ldots, N,$$

where $H_0^{(1)}$ is a Hankel function of the first kind of order zero. In terms of the fundamental solution, we define the single-layer potential

$$u_0(x) = \int_{\Gamma_0} G_0(x,y)\varphi_0(y)\,\mathrm{d}y + \sum_{k=1}^{N} \int_{\Gamma_k} G_0(x,y)\varphi_k(y)\,\mathrm{d}y, \quad x \in \Omega_0, \tag{5}$$

$$u_k(x) = \int_{\Gamma_k} G_k(x,y)\varphi_{N+k}(y)\,\mathrm{d}y, \quad x \in \Omega_k. \tag{6}$$

On page 108 of [14], authors proposed an interior Dirichlet problem in a bounded domain D. They applied a double-layer potential to determine the solution of the interior Dirichlet problem with a continuous density φ. Then, given a continuous function f on the boundary, by the jump relations of Theorem 3.1 of [14], the density φ can be obtained from the integral equation $\varphi - K\varphi = -2f$ on the boundary. If k^2 is not a Dirichlet eigenvalue for D, i.e., the homogeneous Dirichlet problem in D has only the trivial solution, then with the aid of the jump relations it can be seen that $I - K$ has a trivial null space in $C(\partial D)$, for details see [13]. Hence, by Riesz-Fredholm theory $I - K$ has a bounded inverse $(I - K)^{-1}$ from $C(\partial D)$ into $C(\partial D)$. Then they got the uniqueness result in Theorem 5.4 in [14].

In this paper, we try to employ the same method to get the unknown densities φ_k. According to interface conditions (4), we can obtain the Neumann data g_k on the boundary Γ_k. From Theorem 3.1 of [14], we use single-layer potentials to find solutions to the Helmholtz equation in a bounded domain Ω_k with continuous densities φ_k. If we assume that q_k is not a Dirichlet eigenvalue in Ω_k, then based on Riesz-Fredholm theory, the unknown densities φ_k can be got from the integral

equation on Γ_k as follows:

$$\sum_{l=0}^{N}\int_{\Gamma_l}\frac{\partial G_0(x,y)}{\partial\nu(x)}\varphi_l(y)\,\mathrm{d}y+\frac{1}{2}\varphi_k(x)=g_k,\quad k=0,1,\ldots,N,\ x\in\Gamma_k, \tag{7}$$

$$\int_{\Gamma_k}\frac{\partial G_k(x,y)}{\partial\nu(x)}\varphi_{N+k}(y)\,\mathrm{d}y+\frac{1}{2}\varphi_{N+k}(x)=g_{N+k},\quad k=1,\ldots,N,\ x\in\Gamma_k. \tag{8}$$

Let

$$(T_{k,l}\varphi_l)(x)=2\int_{\Gamma_l}\frac{\partial G_0(x,y)}{\partial\nu(x)}\varphi_l(y)\,\mathrm{d}y,\quad x\in\Gamma_k, \tag{9}$$

$$(T_{N+l,N+l}\varphi_{N+l})(x)=2\int_{\Gamma_k}\frac{\partial G_k(x,y)}{\partial\nu(x)}\varphi_{N+l}(y)\,\mathrm{d}y,\quad x\in\Gamma_k. \tag{10}$$

Based on (9)–(10), (7)–(8) can be rewritten as

$$(I+A)\Psi=R, \tag{11}$$

where I is an identity operator, $\Psi=(\varphi_0,\varphi_1,\ldots,\varphi_N,\varphi_{N+1},\ldots,\varphi_{2N})$, $R=2(g_0,g_1,\ldots,g_N,g_{N+1},\ldots,g_{2N})$, and

$$A=\begin{bmatrix}
T_{0,0} & T_{0,1} & \ldots & T_{0,N} & 0 & 0 & \ldots & 0\\
T_{1,0} & T_{1,1} & \ldots & T_{1,N} & 0 & 0 & \ldots & 0\\
 & & \ddots & \vdots & & \ddots & & \\
T_{N,0} & T_{N,1} & \ldots & T_{N,N} & 0 & 0 & \ldots & 0\\
0 & 0 & \ldots & 0 & T_{N+1,N+1} & 0 & \ldots & 0\\
0 & 0 & \ldots & 0 & 0 & T_{N+2,N+2} & \ldots & 0\\
 & & \ddots & & \ddots & \ddots & \ddots & \\
0 & 0 & \ldots & 0 & 0 & 0 & \ldots & T_{2N,2N}
\end{bmatrix}. \tag{12}$$

To our knowledge, operators $T_{k,k}(k=0,1,\ldots,2N)\colon C(\Gamma_k)\to C(\Gamma_k)$ are compact operators [14]. Other operators in matrix A are integral operators with continuous kernels which are compact operators in the corresponding space. In other words, each element of matrix A is a compact operator, thus the matrix A is a compact operator. Hence, by Riesz-Fredholm theory $I+A$ has a bounded inverse $(I+A)^{-1}$. This implies solvability and well-posedness of the interior Dirichlet problem. From the uniqueness result in Theorem 5.4 in [14], we know that we can get the uniqueness for densities in (5)–(6).

This inverse problem is to detect the number, the location and the size of inhomogeneous media within a body, and then try to reconstruct the shape of inhomogeneous

media. In practical problems, we can only get the measurement data g^δ which is an approximation of g satisfying

$$\|g^\delta - g\|_{L^2(\Gamma_0)} \leqslant \delta, \tag{13}$$

where $\|\cdot\|$ denotes the L^2-norm and the constant $\delta > 0$ represents a noisy level.

3. Parametrization

In this section, we want to parameterize the boundary Γ_k of Ω_k. In order to detect the number, the size and the location of inhomogeneous media, we parameterize the boundary Γ_k of Ω_k using the polar coordinate as follows:

$$\Gamma_k\colon\ O_k + \varrho_k(\cos t, \sin t), \quad 0 \leqslant t < 2\pi,$$

where $O_k = (O_{k,1}, O_{k,2})$ is the centroid of the domain Ω_k and ϱ_k is the radius.

If $z_k(t) = (z_{k,1}, z_{k,2}) = \varrho_k(\cos t, \sin t) + O_k$, we have

$$z'_{k,1} = \frac{\mathrm{d}z_{k,1}}{\mathrm{d}t} = -\varrho_k \sin t, \quad z'_{k,2} = \frac{\mathrm{d}z_{k,2}}{\mathrm{d}t} = \varrho_k \cos t.$$

Then we can obtain the outward unit normal

$$\nu(z_k(t)) = \frac{(z'_{k,2}, -z'_{k,1})}{\sqrt{(z'_{k,1})^2 + (z'_{k,2})^2}} = (\cos t, \sin t). \tag{14}$$

We can use $\beta_k = (O_{k,1}, O_{k,2}, \varrho_k)$ to describe the location and the size of inhomogeneous media within a body.

In order to reconstruct the shape of inhomogeneous media, we assume that the subdomain Ω_k is starlike and the boundary Γ_k of Ω_k can be parameterized as

$$\Gamma_k\colon\ O_k + r_k(t)(\cos t, \sin t), \quad 0 \leqslant t \leqslant 2\pi,$$

where O_k is the centroid of the domain Ω_k which is fixed, and $r_k(t)$ a real-valued function of $0 \leqslant t \leqslant 2\pi$ given by the formula

$$r_k(t) = c_{k,0} + \sum_{j=1}^{l_k} (c_{k,j} \cos(jt) + c_{k,j+l_k} \sin(jt)), \tag{15}$$

where $c_{k,j} \in \mathbb{R}$, $l_k \in \mathbb{N}$.

Similarly, let $z_k(t) = (z_{k,1}, z_{k,2}) = r_k(t)(\cos t, \sin t) + O_k$, then

$$z'_{k,1} = \frac{\mathrm{d}z_{k,1}}{\mathrm{d}t} = r'_k(t)\cos t - r_k(t)\sin t,$$
$$z'_{k,2} = \frac{\mathrm{d}z_{k,2}}{\mathrm{d}t} = r'_k(t)\sin t + r_k(t)\cos t.$$

Thus we get the outward unit normal vector

$$\nu(z_k(t)) = \frac{(z'_{k,2}, -z'_{k,1})}{\sqrt{(z'_{k,1})^2 + (z'_{k,2})^2}}. \tag{16}$$

We can use $\beta_k = (c_{k,0}, c_{k,1}, \ldots, c_{k,2l_k})$ to describe the shape of inhomogeneous media within a body.

We proceed by describing the parametrization of the integral equation (5)–(6). For simplification, we assume the boundary Γ_0 is the unit circle whose center is the origin and set $\varphi_k(\tau) = \varphi_k(x_k(\tau))$ for $k = 0, \ldots, 2N$. Thus we get

$$\begin{aligned} u_0(z_{k_1}(t)) = {} & \int_0^{2\pi} G_0(z_{k_1}(t), z_0(\tau))\varphi_0(\tau)\,\mathrm{d}\tau \\ & + \sum_{k=1}^{N} \int_0^{2\pi} G_0(z_{k_1}(t), z_k(\tau))\varphi_k(\tau)|z'_k(\tau)|\,\mathrm{d}\tau, \quad k_1 = 0, 1, \ldots, N, \end{aligned} \tag{17}$$

and

$$u_k(z_k(t)) = \int_0^{2\pi} G_k(z_k(t), z_k(\tau))\varphi_{N+k}(\tau)|z'_k(\tau)|\,\mathrm{d}\tau, \quad k = 1, \ldots, N, \tag{18}$$

where $\varphi_k(\tau)$ $(k = 0, 1, \ldots, 2N)$ are the unknown densities on the boundary.

Due to the interface conditions (4), we know that the densities $\varphi_k(\tau)$, $k = 0, 1, \ldots, 2N$ are the solutions of the system of integral equations

$$\int_0^{2\pi} G_0(z_0(t), z_0(\tau))\varphi_0(\tau)\,\mathrm{d}\tau + \sum_{k=1}^{N} \int_0^{2\pi} G_0(z_0(t), z_k(\tau))\varphi_k(\tau)|z'_k(\tau)|\,\mathrm{d}\tau = f, \tag{19}$$

$$\begin{aligned} & \int_0^{2\pi} G_0(z_{k_1}(t), z_0(\tau))\varphi_0(\tau)\,\mathrm{d}\tau + \sum_{k=1}^{N} \int_0^{2\pi} G_0(z_{k_1}(t), z_k(\tau))\varphi_k(\tau)|z'_k(\tau)|\,\mathrm{d}\tau \\ & \quad - \int_0^{2\pi} G_{k_1}(z_{k_1}(t), z_{k_1}(\tau))\varphi_{N+k_1}(\tau)|z'_{k_1}(\tau)|\,\mathrm{d}\tau = 0, \quad k_1 = 1, \ldots, N, \end{aligned} \tag{20}$$

$$
\begin{aligned}
(21)\quad & \int_0^{2\pi} \frac{\partial G_0(z_{k_2}(t), z_0(\tau))}{\partial \nu(z_{k_2}(t))} \varphi_0(\tau)\,\mathrm{d}\tau + \sum_{k=1}^{N} \int_0^{2\pi} \frac{\partial G_0(z_{k_2}(t), z_k(\tau))}{\partial \nu(z_{k_2}(t))} \varphi_k(\tau) |z_k'(\tau)|\,\mathrm{d}\tau \\
& + \frac{1}{2}\varphi_{k_2}(t) - \int_0^{2\pi} \frac{\partial G_{k_2}(z_{k_2}(t), z_{k_2}(\tau))}{\partial \nu(z_{k_2}(t))} \varphi_{N+k_2}(\tau) |z_{k_2}'(\tau)|\,\mathrm{d}\tau \\
& - \frac{1}{2}\varphi_{N+k_2}(t) = 0, \quad k_2 = 1, \ldots, N.
\end{aligned}
$$

For the discretization of the integral equations, we note that the kernels of the second term, the first term and the first term on the right-hand side of (19), (20), and (21) are smooth so that the trapezoidal rule can be employed for numerical approximation. However, the kernels of the first term, the second, and the third terms on the right-hand side of (19), (20) have singularities [18]. Let

$$
M(t,\tau) = G_k(z(t), z(\tau)) = \frac{\mathrm{i}}{4} H_0^{(1)}(\sqrt{q_k}|z(t) - z(\tau)|)
$$

for $t \neq \tau$; we split it into

$$
M(t,\tau) = M_1(t,\tau) \ln\Big(4 \sin^2 \frac{t-\tau}{2}\Big) + M_2(t,\tau),
$$

where

$$
M_1(t,\tau) := -\frac{1}{4\pi} J_0(\sqrt{q_k}|z(t) - z(\tau)|)
$$

and the diagonal term for M_2 is given by

$$
M_2(t,t) = \frac{\mathrm{i}}{4} - \frac{E}{2\pi} - \frac{1}{4\pi} \ln\Big(\frac{q_k}{4}|z'(t)|^2\Big),
$$

where E denotes Euler constant. The kernels of the second and the fourth terms on the right-hand side of (21) have singularities. Let

$$
L(t,\tau) = -\frac{\mathrm{i}\sqrt{q_k}}{4} H_1^{(1)}(\sqrt{q_k}|z(t) - z(\tau)|) \frac{[z'(t)]^\perp \cdot [z(t) - z(\tau)]}{|z(t) - z(\tau)|},
$$

which can be decomposed in the form

$$
L(t,\tau) = L_1(t,\tau) \ln\Big(4 \sin^2 \frac{t-\tau}{2}\Big) + L_2(t,\tau),
$$

where

$$
L_1(t,\tau) = \frac{\sqrt{q_k}}{4\pi} J_1(\sqrt{q_k}|z(t) - z(\tau)|) \frac{[z'(t)]^\perp \cdot [z(t) - z(\tau)]}{|z(t) - z(\tau)|},
$$

and note that the diagonal term $L_2(t,t)$ is given by

$$
L_2(t,t) = \frac{[z'(t)]^\perp \cdot z''(t)}{4\pi |z'(t)|^2}.
$$

Thus the trapezoidal rule can be employed to the integral equation (19), (20), and (21) for numerical approximation.

Taking into account the density $\varphi_k(\tau)$, $k = 0, 1, \ldots, 2N$, we can obtain the Neumann data on the boundary Γ_0 according to (5):

$$g = \int_0^{2\pi} \frac{\partial G_0(z_0(t), z_0(\tau))}{\partial \nu(z_0(t))} \varphi_0(\tau)\, \mathrm{d}\tau + \frac{1}{2}\varphi_0(t) + \sum_{k=1}^{N} \int_0^{2\pi} \frac{\partial G_0(z_0(t), z_k(\tau))}{\partial \nu(z_0(t))} \varphi_k(\tau) |z_k'(\tau)|\, \mathrm{d}\tau. \tag{22}$$

4. Reconstruction algorithms for the inverse medium problem

In this section, we will apply effective algorithms to determine the salient features of inhomogeneous media. In practical applications, we can only get measured data with errors on the boundary. Inverse medium problem is ill-posed in the sense that the solution does not depend continuously on the input measurement data. Therefore, we should consider regularization techniques for reconstruction algorithms to solve this inverse medium problem.

We consider the cost functional

$$\mathcal{F}(\beta) = \frac{1}{2} \left\| g^{\delta}(z) - \frac{\partial u_0(z, \beta)}{\partial \nu(z)} \right\|^2_{L^2(\Gamma_0)}, \quad z \in \Gamma_0, \tag{23}$$

where u_0 is given by (5), $\|\cdot\|$ denotes the L^2-norm, $g^{\delta}(z)$ are the measured data on the boundary Γ_0, and

$$\beta = (O_{1,1}, O_{1,2}, \varrho_1, \ldots, O_{N,1}, O_{N,2}, \varrho_N) \in \mathbb{R}^{3N}$$

or

$$\beta = (c_{1,0}, \ldots, c_{1,2l_1}, \ldots, c_{N,0}, \ldots, c_{N,2l_N}) \in \mathbb{R}^{2(l_1+\ldots+l_N)+1}.$$

We know that this problem is a nonlinear least squares optimization problem for finding the minimum of the objective function in Eq. (23). There are many iterative algorithms to solve this nonlinear least squares problem, all of these minimization algorithms update the parameter values in order to reduce the error of $\mathcal{F}(\beta)$ for every iteration. Starting with an initial guess $\beta^{(0)}$, these algorithms proceed by the iterations

$$\beta^{(s+1)} = \beta^{(s)} + \triangle, \tag{24}$$

where $\triangle$ is the increment vector. Therefore, how to determine the search direction is very important.

4.1. Trust-Region-Reflective algorithm (TRA). TRA is a subspace trust-region method which is based on the interior-reflective Newton method described in [11], [12]. Each iteration involves the approximate solution of a large linear system using the method of preconditioned conjugate gradient. TRA is used to minimize a nonlinear function subject to simple bound. TRA exhibits strong convergence properties and global and second-order convergence.

We consider the cost functional $\mathcal{F}(\beta)$, and the shape derivative with respect to the parameters β is given by

$$\widetilde{\mathcal{F}}'(\beta) = \frac{\partial \nabla_\beta u_0(\cdot, \beta)}{\partial \nu}. \tag{25}$$

Let the increment $\triangle$ be a solution to quadratic subproblem with a bound step:

$$\min_{\triangle \in \mathbb{R}^n} \Big\{ \psi(\Delta) = \widetilde{\mathcal{F}}'(\beta)^{\mathrm{T}} \triangle + \frac{1}{2} \triangle^{\mathrm{T}} M \triangle \colon \ |B\triangle| \leqslant \Lambda \Big\}, \tag{26}$$

where B is a positive diagonal scaling matrix, see [11], [12] for details, and Λ is a positive scalar representing the trust region size, and

$$M(\beta) = \widetilde{\mathcal{F}}'(\beta)^{\mathrm{T}} \widetilde{\mathcal{F}}'(\beta) + B \operatorname{diag}(\widetilde{\mathcal{F}}'(\beta)) \operatorname{diag}(\operatorname{sign}(\widetilde{\mathcal{F}}'(\beta))) B.$$

Based on the initial descent direction $\triangle$, we determine the piecewise linear reflective path $p(\alpha)$. We perform an approximate piecewise line minimization $F(\beta^{(s)} + p(\alpha))$ with respect to α to determine an acceptable stepsize α, see [11] for detail. Then we get $\beta^{(s+1)} = \beta^{(s)} + p(\alpha)$.

Therefore, we can get the final iteration relationship

$$\beta^{(s+1)} = \beta^{(s)} + p(\alpha). \tag{27}$$

4.2. Levenberg-Marquardt algorithm (LMA). LMA is used to solve nonlinear least squares problems [19], [20], [22]. LMA is used in many software applications for solving generic curve-fitting problems. LMA interpolates between the Gauss-Newton algorithm and the method of gradient descent. LMA is more robust than the Gauss-Newton algorithm, which means that in many cases it finds a solution even if it starts very far off the final minimum.

We consider the cost functional $\mathcal{F}(\beta)$, and the shape derivative with respect to the parameter β is given by

$$\widetilde{\mathcal{F}}'(\beta) = \frac{\partial \nabla_\beta u_0(\cdot, \beta)}{\partial \nu}. \tag{28}$$

Therefore, we can get the increment vector $\triangle$ as

$$\triangle = -(\widetilde{\mathcal{F}}'(\beta)^{\mathrm{T}}\widetilde{\mathcal{F}}'(\beta) + \lambda\,\mathrm{diag}(\widetilde{\mathcal{F}}'(\beta)^{\mathrm{T}}\widetilde{\mathcal{F}}'(\beta)))^{-1}\widetilde{\mathcal{F}}'(\beta)^{\mathrm{T}}\gamma(\beta), \tag{29}$$

where $\gamma(\beta) = g^{\delta} - \partial u_0(\cdot,\beta)/\partial\nu$ and λ is the Marquardt parameter.

Marquardt recommended starting with a value λ_0 and a factor $v > 1$, initially setting $\lambda = \lambda_0$ and computing the residual sum of squares $\gamma(\beta)$ after one step from the starting point with $\lambda = \lambda_0$ and secondly with λ/v. If using the Marquardt parameter λ/v results in a reduction in squared residual then this is taken as the new value of λ and the process continues; if using λ/v resulted in a worse residual, but using λ resulted in a better residual, then λ is left unchanged and the new optimum is taken as the value obtained with λ as the Marquardt parameter.

So we can get the final iteration relationship

$$\beta^{(s+1)} = \beta^{(s)} + \alpha\triangle, \tag{30}$$

where α is the step size of iteration.

5. Numerical experiments

In this section, we present several numerical examples to illustrate the effectiveness of the proposed reconstruction algorithms. All numerical results show that the proposed numerical approaches are feasible and stable.

The noisy measured data are generated by

$$g^{\delta} = g(1 + \delta \cdot \mathrm{rand}(\mathrm{size}(g)),$$

where g is the exact data, $\mathrm{rand}(\mathrm{size}(g))$ is a random number uniformly distributed in $[-1, 1]$ and the magnitude δ indicates a relative noise level.

5.1. Estimation of the number. We explain the procedure of estimating the number of inhomogeneous media within a body. In many applications, maybe we do not know the number of inhomogeneous media or take the number as a priori assumptions within a body. Thus it is very important how to detect the number of inhomogeneous media. Our idea is derived from [15]. In [15]; the authors took $M = 10$ possible singular sources, which corresponds to the number of singular values of B. We take the threshold value σ, delete the small singular values, and then obtain "usable" point sources. Inspired by the idea of Hanke and Rundell, we try to use the circle to measure the inhomogeneous medium. If the radius of a circle becomes

very small which is less than the threshold value along with iterations, we take the circle as "unusable" and delete it in terms of the threshold value. In addition, if the distance between two circles is less than the threshold value, we take the two circles as an inhomogeneous medium.

In order to obtain the number of inhomogeneous media, we parameterize the boundary Γ_k of Ω_k as $O_k + \varrho_k(\cos t, \sin t)$, $0 \leqslant t \leqslant 2\pi$, along with $\beta = (O_{k,1}, O_{k,2}, \varrho_k)$. First, for a given estimate of the level of noise in g^δ, we estimate a threshold value of the lower bound ε^δ. The circle should not be viewed as an inhomogeneous medium whose value of radius is less than ε^δ. Secondly, consider a set of circles $\{O_k\}$, $k \in \mathbb{Z}^+$. If for every $k_1 \in \mathbb{Z}^+$ there exists a $k_2 \in \mathbb{Z}^+$ such that the distance between the two circles satisfies $d(O_{k_1}, O_{k_2}) < \varepsilon^\delta$, we say the circles set $\{O_k\}$ is connected. This connected set is seen as an inhomogeneous medium. Based on these two criteria, we can estimate the number of inhomogeneous media within a body according to the threshold value ε^δ.

E x a m p l e 5.1.1. In this case, we consider one inhomogeneous medium within a body which is a peanut, and we take the centroid as $O_1(0, 0)$ along with $q_0 = 1$ and $q_1 = 2$. The polar radius of a peanut is given by

$$r_{pt} = \tfrac{6}{25}\sqrt{\cos^2 t + \tfrac{1}{4}\sin^2 t}, \quad 0 \leqslant t \leqslant 2\pi.$$

Our initial estimate is to allow $N = 2, 3$ as the possible number of inhomogeneous media within a body.

We apply LMA to determine the number of inhomogeneous media using two or three possible estimates with 1% random noise in the data. We take $\lambda_0 = 0.1$ and $v = 10$, apply $\varrho^{(0)} = 0.03$ as the radius of the starting guess for every inhomogeneous medium, and take $|\mathcal{F}(\beta^{(s+1)}) - \mathcal{F}(\beta^{(s)})| < 10^{-3}$ as a stopping criterion of iterations. Then, we can update $\beta^{(s)}$ for every iteration step.

Figure 2 and Table 1, compared with the recovered radii for each case, enable us to determine the number $M = 1$ of the medium when we take the threshold value $\varepsilon^\delta = 0.04, 0.02$ for Figures 2(b) and 2(d), respectively. However, from Figures 2(a) and 2(c), we can see that the sets $\{O_1, O_2\}$ cover the square, hence are recognized as connected. Thus we can take arbitrarily small positive number ε^δ as the threshold value. Applying the above proposed two criteria, it is easy to determine the number of inhomogeneous media within a body.

E x a m p l e 5.1.2. In this case, we consider two inhomogeneous media within a body which are a pear and a bean, and we take $q_0 = 1$ and $q_1 = q_2 = 2$. The polar radius of a pear is given by

$$r_{pr} = 0.3(\tfrac{6}{25} + \tfrac{1}{20}\cos(3t)), \quad 0 \leqslant t \leqslant 2\pi,$$

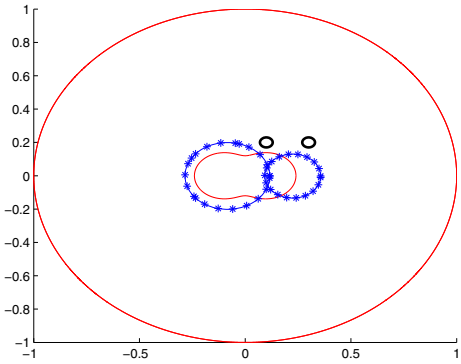

(a) $\lambda = 0.1$, $\alpha =$ 3.8146e-8

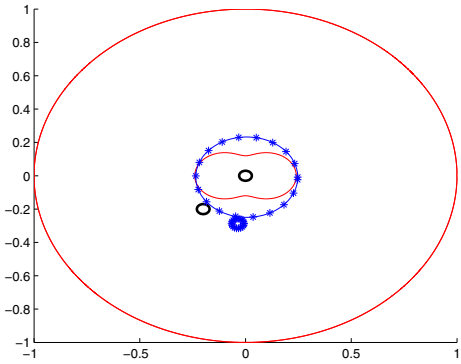

(b) $\lambda = 0.001$, $\alpha =$ 4.1002e-12

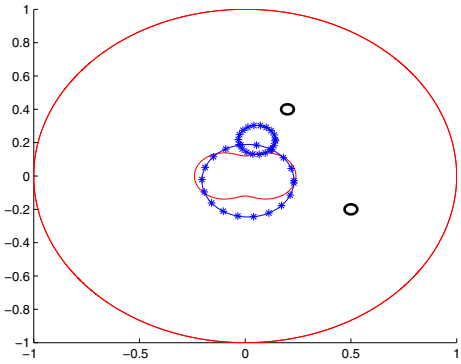

(c) $\lambda = 0.001$, $\alpha =$ 1.2172e-7

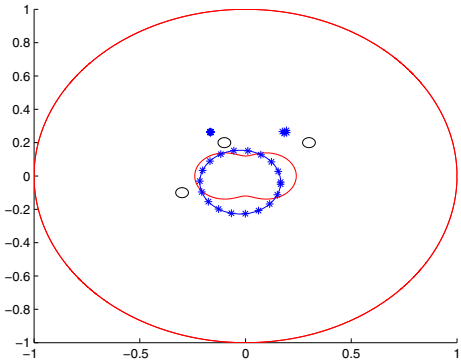

(d) $\lambda = 0.1$, $\alpha = 0.0432$

Figure 2. Detecting the number of inhomogeneous media using two or three possible estimates with 1% noise data along with the exact solution (Red, Solid), initial guess (Black, Solid, Bold) and the recovered solution (Blue, Solid, $*$), respectively, for Example 5.1.1.

ϱ	ϱ_1	ϱ_2	ϱ_3
(a)	0.1066	0.2193	–
(b)	0.0351	0.2219	–
(c)	0.0664	0.2012	–
(d)	0.0015	0.1911	0.0111

Table 1. The reconstructed radius ϱ of different cases with $N = 2, 3$ in Figure 2 for Example 5.1.1.

and the polar radius of a bean is parameterized by

$$r_{bn} = 0.1(\tfrac{1}{5} + \tfrac{9}{50}\cos t + \tfrac{3}{100}\sin(2t))/(1 + \tfrac{7}{10}\cos t), \quad 0 \leqslant t \leqslant 2\pi.$$

Our initial estimate is to allow $N = 3$ as the possible number of inhomogeneous media within a body.

In this example, we consider how to determine the number for a multiscale medium problem. In Figures 3(a) and 3(b) with the same exact solutions along with different locations. The locations lie in $(-0.2, 0.4)$, $(0.3, -0.3)$ and $(0, 0)$, $(0.3, -0.3)$ for Figures 3(a) and 3(b), respectively. We take 40 measured data along with 1% noise level. In Figure 3(a), the pear is large and the bean is small, moreover the pear is far from the bean, which can be viewed as two inhomogeneous media. From Figure 3(a) and Table 2(a), we can determine the number $M = 2$ of media according to the above second criterion. In Figure 3(b), the pear is very closed to the bean which can be viewed as an inhomogeneous medium. From Figure 3(b) and Table 2(b), we can determine the number $M = 1$ of inhomogeneous media according to the above two criteria along with $\varepsilon^\delta = 0.02$.

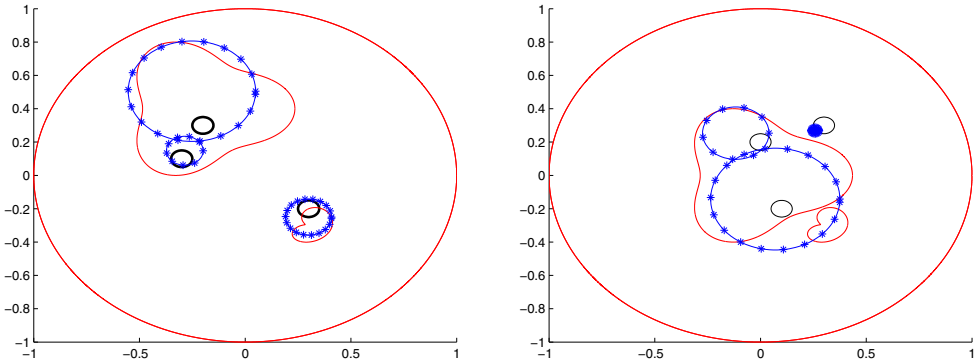

(a) $\lambda = 0.01$, $\alpha = 0.0813$ (b) $\lambda = 0.1$, $\alpha = 1.0174\text{e-}012$

Figure 3. Detecting the number of inhomogeneous media using two or three possible estimates with 1% noise data along with the exact solution (Red, Solid), initial guess (Black, Solid, Bold) and the recovered solution (Blue, Solid, $*$), respectively, for Example 5.1.2.

ϱ	ϱ_1	ϱ_2	ϱ_3
(a)	0.3002	0.1706	0.0856
(b)	0.1570	0.0197	0.3054

Table 2. The reconstructed radius ϱ of different cases in Figure 3 for Example 5.1.2.

5.2. Estimation of the location and the size of inhomogeneous media. In order to estimate the location and the size of inhomogeneous media within a body, we parameterize the boundary Γ_k of Ω_k as $O_k + \varrho_k(\cos t, \sin t)$, $0 \leqslant t \leqslant 2\pi$, along with $\beta = (O_{k,1}, O_{k,2}, \varrho_k)$, that is, we use the circle to approximate the inhomogeneous medium for every iteration.

E x a m p l e 5.2.1. In this case, we suppose the inhomogeneous medium is a peanut or a peach or a pear or a bean which is located in $(0.1, 0.3)$ along with $q_0 = 1$ and

$q_1 = 2$. The polar radius of a peanut is parameterized by

$$r_{pt} = \tfrac{8}{25}\sqrt{\cos^2 t + \tfrac{1}{4}\sin^2 t}, \quad 0 \leqslant t \leqslant 2\pi,$$

the polar radius of a peach is parameterized by

$$r_{ph} = \tfrac{6}{25} - \tfrac{1}{15}\sin t - \tfrac{1}{35}\sin(3t), \quad 0 \leqslant t \leqslant 2\pi,$$

the polar radius of a pear is parameterized by

$$r_{pr} = \tfrac{6}{25} + \tfrac{1}{20}\cos(3t), \quad 0 \leqslant t \leqslant 2\pi,$$

and the polar radius of a bean is parameterized by

$$r_{bn} = (\tfrac{1}{5} + \tfrac{9}{50}\cos t + \tfrac{3}{100}\sin(2t))/(1 + \tfrac{7}{10}\cos t), \quad 0 \leqslant t \leqslant 2\pi.$$

In Figures 4, we can get the approximate centroid location and the size of the inhomogeneous medium within a body using LMA with 1% noise data. In our experiment, we can use any point and any radius as a starting guess in the domain of the solution for these four cases. In Figures 4, we take $\lambda_0 = 0.05$ and $v = 10$, choose $(0.4, 0.1, 0.07)$ as a test for starting guess, and take $|\mathcal{F}(\beta^{(s+1)}) - \mathcal{F}(\beta^{(s)})| < 10^{-5}$ as a stopping criterion of iterations. From Figures 4 and Table 3, it can be seen that we get a more accurate approximation of the location and the size for four different cases. We can get the same results when using TRA to recover the location and the size of the inhomogeneous medium within a body.

LS_E	(0.1,0.3,r)
LS_{SG}	(0.4,0.1,0.07)
(a)	(0.1196,0.3096,0.2277)
(b)	(0.1010,0.2418,0.2388)
(c)	(0.0773,0.3012,0.2510)
(d)	(0.1617,0.2951,0.2031)

Table 3. The approximate location and the size of the inhomogeneous media using TRA with exact solution (LS_E) and the starting guess (LS_{SG}) along with 1% noise data for Example 5.2.1.

5.3. Estimation of the shape of inhomogeneous media. From the previous two subsections, we know that the number, the location and the size of inhomogeneous media can be determined. In the following, we try to recover the shape of inhomogeneous media along with the number, the location and the size given a priori. Therefore, We can parameterize the boundary Γ_k of Ω_k as $r_k(t)(\cos t, \sin t) + O_k$

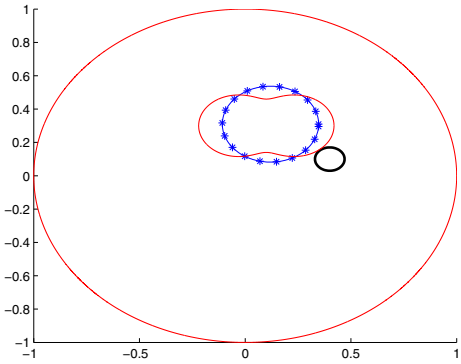

(a) $\lambda = 5\text{e-}7$, $\alpha = 3.1548\text{e-}5$

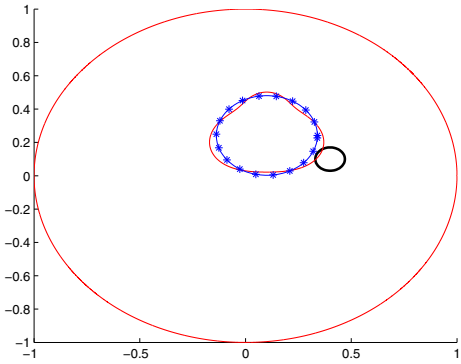

(b) $\lambda = 5\text{e-}5$, $\alpha = 2.1386\text{e-}5$

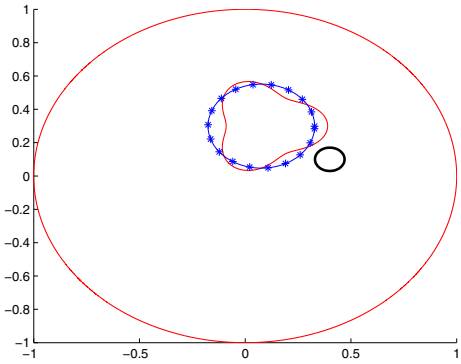

(c) $\lambda = 5\text{e-}5$, $\alpha = 1.9637\text{e-}5$

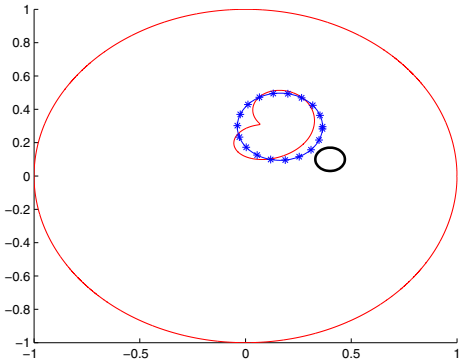

(d) $\lambda = 5\text{e-}7$, $\alpha = 7.3365\text{e-}6$

Figure 4. (a) peanut; (b) peach; (c) pear; (d) bean. Estimate the location and the size of the inhomogeneous medium with 1% noise data along with exact solution (Red, Solid), initial guess (Black, Solid, Bold) and recovered solution (Blue, Solid, $*$), respectively, for Example 5.2.1.

with $r_k(t)$ a real-valued function of $0 \leqslant t \leqslant 2\pi$, and O_k the fixed center of the inhomogeneous medium Ω_k. We apply LMA and TRA to reconstruct the shape of inhomogeneous media.

In order to quantify the accuracy between such parametric forms of shape and the exact ones, we take the Hausdorff distance as a nice tool to present such accuracy. Let X and Y be two nonempty subsets of a metric space. We define their Husdorff distance $d_H(X, Y)$ by

$$d_H(X, Y) = \max\Big\{ \sup_{x\in X} \inf_{y\in Y} d(x, y), \sup_{y\in Y} \inf_{x\in X} d(x, y)\Big\},$$

where sup represents the supremum and inf the infimum.

The Hausdorff distance, or Hausdorff metric, also called Pompeiu-Hausdorff distance, measures how far two subsets of a metric space are from each other. Informally,

two sets are close in the Hausdorff distance if every point of either set is close to some point of the other set. The Hausdorff distance is the longest distance you can be forced to travel by an adversary who chooses a point in one of the two sets, from where you then must travel to the other set. In other words, it is the greatest of all the distances from a point in one set to the closest point in the other set.

E x a m p l e 5.3.1. In this case, we want to show the stability of our proposed reconstruction algorithms. We assume the inhomogeneous medium is a peanut which is located in $(0.1, 0.3)$ along with $q_0 = 1$ and $q_1 = 2$. The polar radius of the peanut is given in Example 5.2.1.

In Figure 5, we employ LMA to reconstruct the shape of the inhomogeneous medium within a homogeneous medium along with $\delta = 1\%, 5\%, 10\%, 15\%$, respectively. We take $l = 2$, $\lambda_0 = 0.001$, $v = 10$, choose $c_0^{(0)} = 0.01$ as a starting guess, and take $|\mathcal{F}(\beta^{(s+1)}) - \mathcal{F}(\beta^{(s)})| < 10^{-5}$ as a stopping criterion of iterations. In Figure 5,

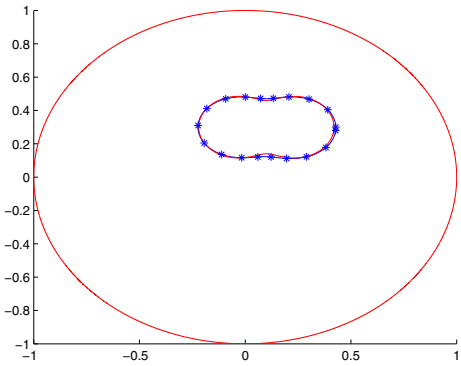

(a) $\delta = 1\%$, $\lambda =$ 1e-5, $\alpha =$ 3.37e-6

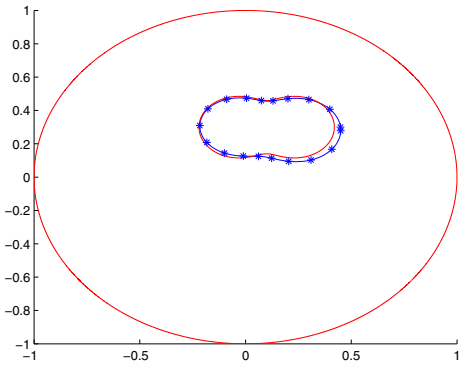

(b) $\delta = 5\%$, $\lambda =$ 1e-5, $\alpha =$ 3.28e-6

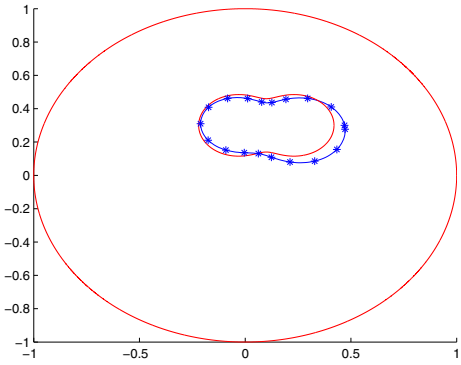

(c) $\delta = 10\%$, $\lambda =$ 1e-4, $\alpha =$ 3.32e-5

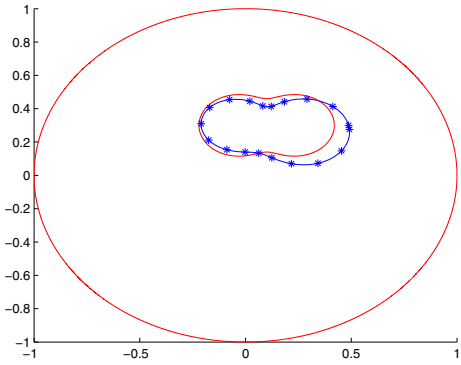

(d) $\delta = 15\%$, $\lambda =$ 1e-4, $\alpha =$ 6.04e-4

Figure 5. Using LMA to estimate the shape of the inhomogeneous medium with four different noise levels along with the exact solution (Red, Solid) and the recovered solution (Blue, Solid, $*$), respectively, for Example 5.3.1.

the Hausdorff distances are 0.0173, 0.0351, 0.0618, 0.0830 for Figures 5(a), 5(b), 5(c) and 5(d) along with $\delta = 1\%$, 5%, 10%, 15%, respectively. From Figure 5, it can be seen that we can reconstruct the approximate shape of the inhomogeneous medium within a body for four different noise levels. The smaller the error, the better the result. The reconstruction results show that our proposed reconstruction algorithm is stable. TRA can get the same results as LMA.

E x a m p l e 5.3.2. In this case, we also assume the inhomogeneous medium is a peanut or a peach or a pear or a bean with the approximate location and the size given in Table 3 in Example 5.2.1.

From Table 3 in Example 5.2.1, we know the approximate location and the size of the inhomogeneous medium for four different cases. In the following, we consider to recover the shape of the inhomogeneous medium. We fix the location of the inhomogeneous medium, take $\lambda_0 = 0.05$ and $v = 10$, choose $|\mathcal{F}(\beta^{(s+1)}) - \mathcal{F}(\beta^{(s)})| < 10^{-5}$ as a stopping criterion of iterations, and take the size as a starting guess $c_0^{(0)} = \varrho$, referring to Table 3 in Example 5.2.1, then we use TRA and LMA to reconstruct the shape of the inhomogeneous medium within a homogeneous medium. In Figure 6, the Hausdorff distances are 0.0244, 0.0249, 0.0466, 0.0769 for Figures 6(a), 6(b), 6(c), and 6(d), respectively. In Figure 7, the Hausdorff distances are 0.0244, 0.0249, 0.0636, 0.0767 for Figures 7(a), 7(b), 7(c) and 7(d), respectively. From Figures 6 and 7, it can be seen that we can get a more accurate shape of the inhomogeneous medium within a body.

E x a m p l e 5.3.3. In this case, we consider two inhomogeneous media within a body which are a peanut and a circle. The peanut is located in $(-0.2, 0.4)$ along with $q_0 = 1$ and $q_1 = 2$ and its polar radius is parameterized by

$$r_{pt} = \tfrac{4}{25}\sqrt{\cos^2 t + \tfrac{1}{4}\sin^2 t}, \quad 0 \leqslant t \leqslant 2\pi.$$

The circle is located in $(0.3, -0.3)$ along with $q_2 = 3$ and its radius is 0.2.

In this example, we try to reconstruct two inhomogeneous media using TRA and LMA. We take $\lambda_0 = 0.001$, $v = 10$, $l_1 = 2$ and $l_2 = 1$, choose $c_0^{(0)} = 0.1$ as the starting guess, and take $|\mathcal{F}(\beta^{(s+1)}) - \mathcal{F}(\beta^{(s)})| < 10^{-2}$ as a stopping criterion of iterations. In our experiment, we take the parameters $\lambda =$ 1e-11 and $\alpha = 0.0022$. In Figure 8(a), we can obtain the Hausdorff distance $d_H = 0.0212$, 4.0e-4 for peanut and circle, respectively. Thus we can use one Hausdorff distance $d_H = 0.0212$ to quantify the accuracy of a multiscale medium. For Figure 8(b), we can get the same conclusion for the Hausdorff distance $d_H = 0.0332$. From Figure 8, we can see that our proposed algorithms can get a more accurate shape of two inhomogeneous media within a body.

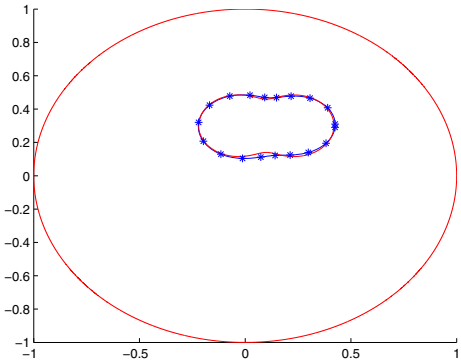

(a) $c_0^{(0)} = 0.2277$, $l = 2$, $d_H = 0.0244$

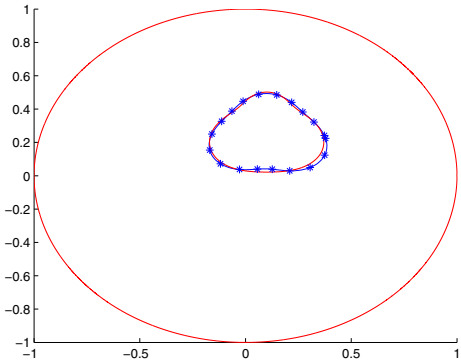

(b) $c_0^{(0)} = 0.2388$, $l = 3$, $d_H = 0.0249$

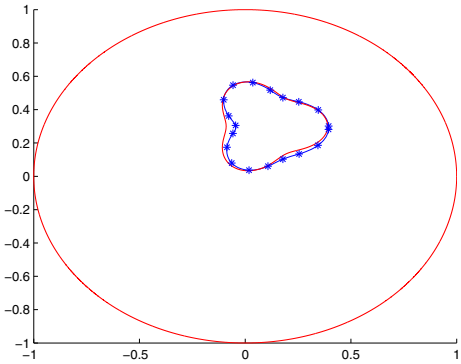

(c) $c_0^{(0)} = 0.2510$, $l = 3$, $d_H = 0.0466$

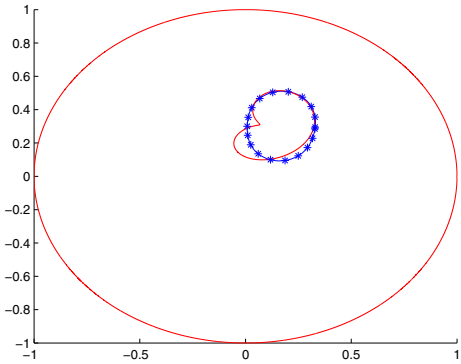

(d) $c_0^{(0)} = 0.2031$, $l = 2$, $d_H = 0.0769$

Figure 6. (a) peanut; (b) peach; (c) pear; (d) bean. Using TRA to estimate the shape of the inhomogeneous medium with 1% noise data along with the exact solution (Red, Solid) and the recovered solution (Blue, Solid, $*$), respectively, for Example 5.3.2.

E x a m p l e 5.3.4. In this case, we also consider two inhomogeneous media within a body which are a pear and a circle. The pear is located in $(-0.2, 0.4)$ along with $q_0 = 1$ and $q_1 = 2$ and its polar radius is parameterized by

$$r_{pr} = \tfrac{18}{125} + \tfrac{3}{100}\cos(3t), \quad 0 \leqslant t \leqslant 2\pi, \ 0 \leqslant t \leqslant 2\pi.$$

The circle is located in $(0.3, -0.3)$ along with $q_2 = 2$ and its radius is 0.2.

We try to reconstruct two inhomogeneous media using TRA and LMA in this example. We take $\lambda_0 = 0.001$, $v = 10$, $l_1 = 3$, and $l_2 = 1$, choose $c_0^{(0)} = 0.1$ as the starting guess, and take $|\mathcal{F}(\beta^{(s+1)}) - \mathcal{F}(\beta^{(s)})| < 10^{-2}$ as a stopping criterion of iterations. In our experiment, we take the parameters $\lambda =$ 1e-14 and $\alpha = 0.0041$. In Figures 9(a) and 9(b), we obtain the Hausdorff distances $d_H = 0.0430$, 0.0382 to quantify the accuracy of multiscale media, respectively. From Figure 9, we know that the results match the exact ones very well.

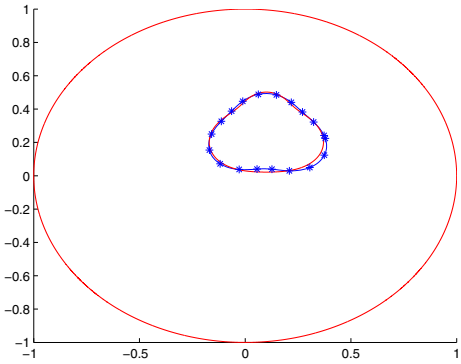

(a) $\lambda =$ 5e-5, $\alpha =$ 3.9181e-5

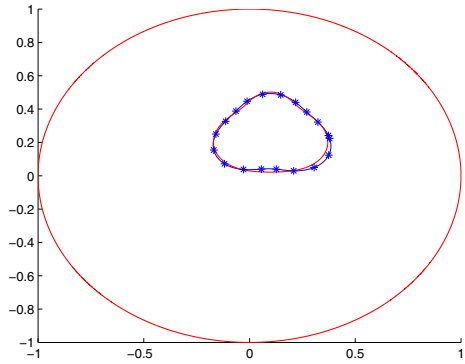

(b) $\lambda =$ 5e-7, $\alpha =$ 6.4963e-5

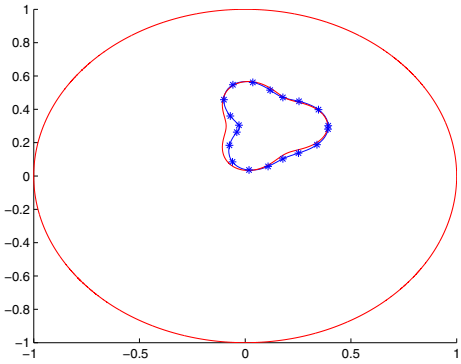

(c) $\lambda =$ 5e-10, $\alpha =$ 3.8785e-4

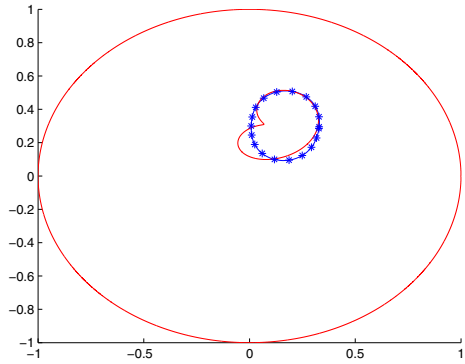

(d) $\lambda =$ 5e-6, $\alpha =$ 9.8193e-5

Figure 7. (a) peanut; (b) peach; (c) pear; (d) bean. Using LMA to estimate the shape of the inhomogeneous medium with 1% noise data along with the exact solution (Red, Solid) and the recovered solution (Blue, Solid, $*$), respectively, for Example 5.3.2.

6. Conclusions

In this paper, we consider an inverse medium problem for the Helmholtz equation. Our goal is to seek simple, convenient and efficient numerical algorithms to detect the number, the location and the size of inhomogeneous media, and then to recover the shape of inhomogeneous media from the noise data on the boundary. This inverse problem is nonlinear and ill-posed. We should employ regularization techniques in our proposed numerical algorithms. We propose both algorithms of TRA and LMA to detect the salient features of inhomogeneous media within a body. Numerical examples show that the proposed numerical approaches are efficient, feasible and stable for reconstructing inhomogeneous media.

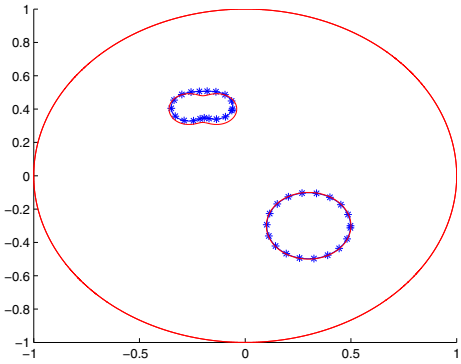
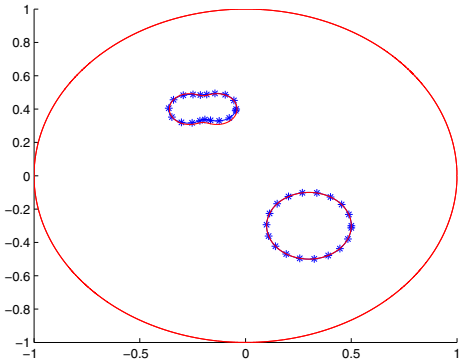

(a) $d_{H_{pt}} = 0.0212$, $d_{H_c} = 4.0\text{e-}4$ (b) $d_{H_{pt}} = 0.0332$, $d_{H_c} = 0.0019$

Figure 8. (a) TRA; (b) LMA. Using TRA and LMA to reconstruct the shape of inhomogeneous media with 1% noise data along with the exact solution (Red, Solid) and the recovered solution (Blue, Solid, $*$), respectively, for Example 5.3.3.

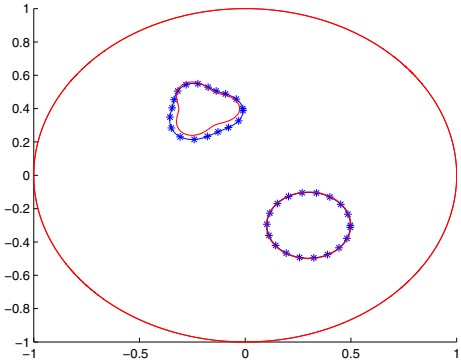
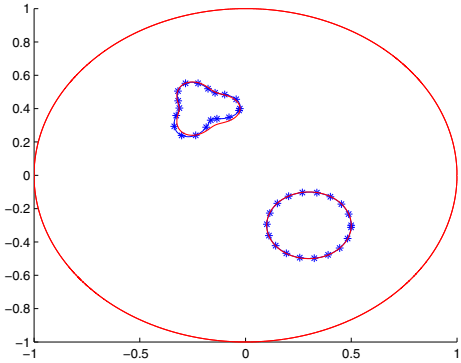

(a) $d_{H_{pr}} = 0.0430$, $d_{H_c} = 0.0027$ (b) $d_{H_{pr}} = 0.0382$, $d_{H_c} = 8.0\text{e-}4$

Figure 9. (a) TRA; (b) LMA. Using TRA and LMA to reconstruct the shape of inhomogeneous media with 1% noise data along with the exact solution (Red, Solid) and the recovered solution (Blue, Solid, $*$), respectively, for Example 5.3.4.

References

[1] *H. Ammari, E. Bonnetier, Y. Capdeboscq, M. Tanter, M. Fink*: Electrical impedance tomography by elastic deformation. SIAM J. Appl. Math. *68* (2008), 1557–1573. zbl MR doi

[2] *H. Ammari, E. Bossy, J. Garnier, L. H. Nguyen, L. Seppecher*: A reconstruction algorithm for ultrasound-modulated diffuse optical tomography. Proc. Am. Math. Soc. *142* (2014), 3221–3236. zbl MR doi

[3] *H. Ammari, E. Bossy, J. Garnier, L. Seppecher*: Acousto-electromagnetic tomography. SIAM J. Appl. Math. *72* (2012), 1592–1617. zbl MR doi

[4] *H. Ammari, Y. Capdeboscq, F. de Gournay, A. Rozanova-Pierrat, F. Triki*: Microwave imaging by elastic deformation. SIAM J. Appl. Math. *71* (2011), 2112–2130. zbl MR doi

[5] *H. Ammari, Y. Capdeboscq, H. Kang, A. Kozhemyak*: Mathematical models and reconstruction methods in magneto-acoustic imaging. Eur. J. Appl. Math. *20* (2009), 303–317. zbl MR doi

[6] *H. Ammari, J. Garnier, L. H. Nguyen, L. Seppecher*: Reconstruction of a piecewise smooth absorption coefficient by an acousto-optic process. Commun. Partial Differ. Equations *38* (2013), 1737–1762. zbl MR doi
[7] *G. Bal, J. C. Schotland*: Inverse scattering and acousto-optic imaging. Phys. Rev. Lett. *104* (2010), Article ID 043902. doi
[8] *G. Bal, G. Uhlmann*: Reconstruction of coefficients in scalar second-order elliptic equations from knowledge of their solutions. Commun. Pure Appl. Math. *66* (2013), 1629–1652. zbl MR doi
[9] *G. Bao, T. Triki*: Error estimates for the recursive linearization of inverse medium problems. J. Comput. Math. *28* (2010), 725–744. zbl MR doi
[10] *M. Choulli, F. Triki*: New stability estimates for the inverse medium problem with internal data. SIAM J. Math. Anal. *47* (2015), 1778–1799. zbl MR doi
[11] *T. F. Coleman, Y. Li*: On the convergence of interior-reflective Newton methods for nonlinear minimization subject to bounds. Math. Program. *67* (1994), 189–224. zbl MR doi
[12] *T. Coleman, Y. Li*: An interior, trust region approach for nonlinear minimization subject to bounds. SIAM J. Optim. *6* (1996), 418–445. zbl MR doi
[13] *D. Colton, R. Kress*: Integral Equation Methods in Scattering Theory. Pure and Applied Mathematics. A Wiley-Interscience Publication. John Wiley & Sons, New York, 1983. zbl MR
[14] *D. Colton, R. Kress*: Inverse Acoustic and Electromagnetic Scattering Theory. Applied Mathematical Sciences 93, Springer, Berlin, 1992. zbl MR doi
[15] *M. Hanke, W. Rundell*: On rational approximation methods for inverse source problems. Inverse Probl. Imaging *5* (2011), 185–202. zbl MR doi
[16] *V. Isakov*: Inverse Problems for Partial Differential Equations. Applied Mathematical Sciences 127, Springer, New York, 2006. zbl MR doi
[17] *K. Ito, B. Jin, J. Zou*: A direct sampling method to an inverse medium scattering problem. Inverse Probl. *28* (2012), Article ID 025003, 11 pages. zbl MR doi
[18] *R. Kress*: Linear Integral Equations. Applied Mathematical Sciences 82, Springer, New York, 1999. zbl MR doi
[19] *K. Levenberg*: A method for the solution of certain non-linear problems in least squares. Q. Appl. Math. *2* (1944), 164–168. zbl MR doi
[20] *D. W. Marquardt*: An algorithm for least-squares estimation of nonlinear parameters. J. Soc. Ind. Appl. Math. *11* (1963), 431–441. zbl MR doi
[21] *W. McLean*: Strongly Elliptic Systems and Boundary Integral Equations. Cambridge University Press, Cambridge, 2000. zbl MR
[22] *J. J. Moré*: The Levenberg-Marquardt algorithm: implementation and theory. Numerical Analysis (G. A. Watson et al., eds.). Lecture Notes in Mathematics 630, Springer, Berlin, 1978, pp. 105–116. zbl MR doi
[23] *J. C. Schotland*: Direct reconstruction methods in optical tomography. Mathematical Modeling in Biomedical Imaging II (H. Ammari et al., eds.). Lecture Notes in Mathematics 2035, Springer, Berlin, 2012, pp. 1–29. zbl MR doi
[24] *J. Sylvester, G. Uhlmann*: A global uniqueness theorem for an inverse boundary value problem. Ann. Math. (2) *125* (1987), 153–169. zbl MR doi
[25] *F. Triki*: Uniqueness and stability for the inverse medium problem with internal data. Inverse Probl. *26* (2010), Article ID 095014, 11 pages. zbl MR doi
[26] *T. Widlak, O. Scherzer*: Stability in the linearized problem of quantitative elastography. Inverse Probl. *31* (2015), Article ID 035005, 27 pages. zbl MR doi

Author's address: *Ji-Chuan Liu*, School of Mathematics, China University of Mining and Technology, Xuzhou, Jiangsu 221116, P. R. China, e-mail: `liujichuan2003@126.com`.